ARCTIC OBSERVATIONS WITH THE UNIVERSITY OF WISCONSIN HIGH SPECTRAL RESOLUTION LIDAR

Edwin W. Eloranta[1] and Taneil Uttal[2]

[1]*University of Wisconsin, 1225 W. Dayton St., Madison, WI, USA, eloranta@lidar.ssec.wisc.edu*
[2]*NOAA Earth Systems Research Laboratory, 325 Broadway, Boulder, CO, USA taneil.uttal@noaa.gov*

ABSTRACT

Measurements from the NOAA SEARCH observatory at Eureka, Canada (80N, 85 W) provide unique Arctic cloud observations. The University of Wisconsin Arctic High Spectral Resolution Lidar and the NOAA 8.6 mm wavelength Doppler radar have provided nearly continuous data since their August 2005 deployment. A prior deployment to Barrow, Alaska(71N, 156W) provided data between August 24 and November 17 of 2004. Particle size and optical depth measurements are presented.

1. INTRODUCTION

Since August 1, 2005 the University of Wisconsin High Spectral Resolution Lidar(HSRL) and the NOAA 8.6 mm wavelength cloud radar (MMCR) have operated in the high Arctic at Eureka, Canada (80N, 85W). In March of 2006 the University of Idaho Polar Atmospheric Emitted Radiance Interferometer (PAERI) was installed at the same location. These instruments are operating as part of the US National Oceanic and Atmospheric Administration (NOAA) SEARCH program. SEARCH seeks to provide continuous measurements of Arctic surface radiation, clouds, aerosols and chemistry sufficient for detailed evaluation of interactive climate change processes in the lower atmosphere.

The University of Wisconsin Arctic High Spectral Resolution Lidar (HSRL) operates as a minimally-tended Internet appliance. An expanded transmitted beam and low pulse energy make the output beam eye safe. The HSRL uses molecular scattering as a calibration reference to provide absolutely calibrated profiles of backscatter cross section, optical depth and depolarization [2; 6; 7]. The MMCR provides calibrated measurements of radar reflectivity, Doppler velocity, and Doppler spectra [3], while the PAERI provides calibrated, high resolution infrared spectra[1].

During the MPACE and SEARCH deployments the HSRL has been programmed to provide profiles with 7.5 m vertical and 2.5 second temporal resolution. Usable data begins at 150 m above the surface and extends to 30 km. Lidar and radar data are posted on our web site: http://lidar.ssec.wisc.edu. Lidar data from altitudes be-
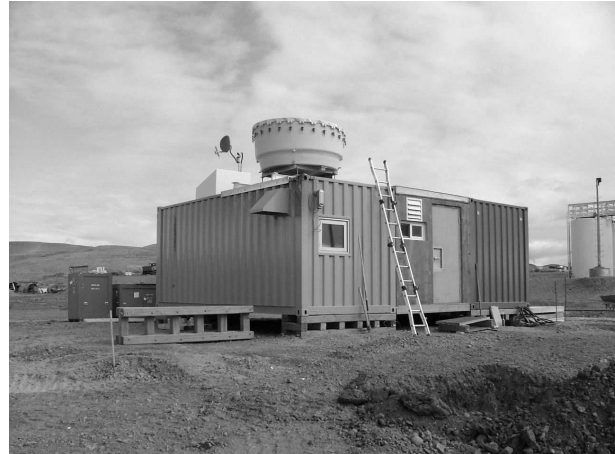

Figure 1. Two seatainers are joined together as shelter for the lidar, radar, and PAREI instruments. The 35 GHz radar antenna is seen on the near corner of the shelter and the zenith facing lidar window is located in the white box directly behind the radar antenna.

low 15 km are posted in real time while the higher altitude data is transfered at approximately monthly intervals. Radar data is recorded with 30 m vertical and 10 second temporal resolution. Radar data is available approximately one day after it is recorded. Quick-look images show all lidar and radar data from one month on a single web page. Images and netcdf download files with user specified averaging, altitude ranges and time intervals can be generated via the web site. Lidar and radar data are presented with common grids allowing easy inter-comparison. Lidar data includes: depolarization, backscatter cross section, scattering cross section, and optical depth along with system housekeeping information. Radar data includes: reflectivity, backscatter cross section, Doppler velocity, and spectral width. Cloud particle effective diameter, number density, and liquid water content are computed using a combination of the lidar and radar data. These are computed following Donovan et at[4]. However, Donovan's iterative solution is not required because HSRL data is corrected for extinction, robustly calibrated, and the HSRL has a 45 micro-radian field-of-view that limits multiple scattering.
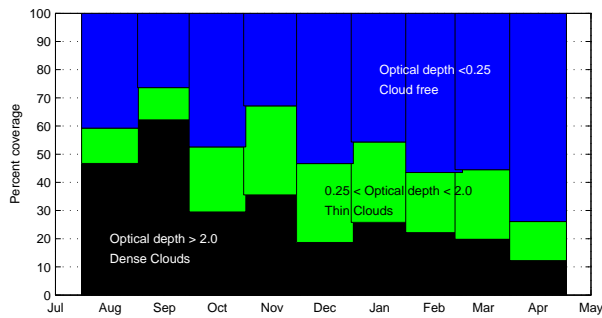
Figure 2. Monthly plot of cloudiness at Eureka for August 8, 2005 to May 1, 2006. Optical depths measured between 150 m and 12 km have been sorted into three cloud categories. Moderate cloud cover in late summer (60%) decreased through the winter leading to a very clear April with a total cloud cover of 26% and dense clouds only 11% of the time.

2.   CLOUD OBSERVATIONS

Considerable uncertainty exists in current satellite derived Arctic cloud climatologies. Visible wavelength satellite data is absent during the long winter and it provides little contrast between the ice covered portions of the ocean and clouds during the summer. Infrared retrievals are hampered by intense low level temperature inversions which make it difficult to assign altitudes and open leads in the ice which make it difficult to specify the surface contribution to the observed radiance. Cloud fraction data from the HSRL in Eureka will provide an important source of validation for satellite climatologies.

Figure 2 shows cloud cover observed at Eureka between August 8, 2005 and May 1, 2006. The HSRL operated nearly continuously. Data collected at 2.5 second intervals was averaged into 3-minute profiles. Each profile was classified according to the optical depth measured
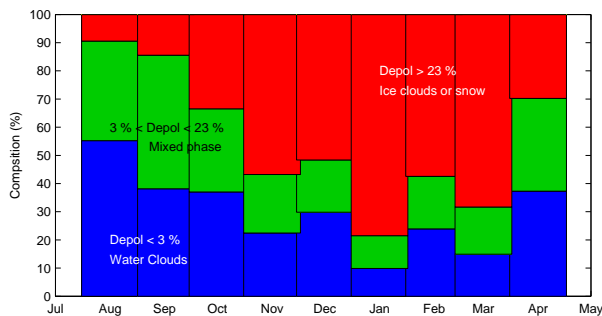

Figure 3. Monthly plot of cloud phase at Eureka for August 8, 2005 to May 1, 2006. This shows the percentage of the optical depth generated by water, ice and mixed phase cloud elements. Phase has been identified from the depolarization of the lidar return.

between altitudes of 150 m and 12 km. Profiles were divided into three optical depth classes: less than 0.25 (cloud free), greater than 2 (dense clouds), and between 0.25 and 2 (thin clouds). Eureka is remarkably cloud free in the winter and early spring. Total cloud cover in April 2006 was only 26% with dense clouds occurring only 11% of the time.
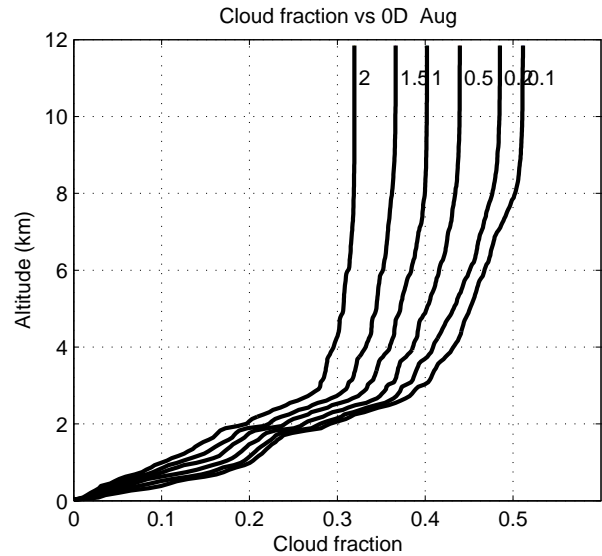

Figure 4. Cloud fraction as a function of altitude for August 2005 in Eureka. Curves show the fraction of the time that the atmosphere is clear up to a given altitude. Separate curves show the effect of changing the optical depth threshold which defines a cloud.

Figure 3 shows a monthly plot of cloud phase for the period shown in figure 2. Clouds were defined as regions with a backscatter cross section of greater than 10^{-6} $m^{-1}sr^{-1}$. The plot shows integrated backscatter cross sections divided by the mean backscatter phase function to provide an estimate of the optical depth encountered by the laser beam. This has been sorted into three categories depending on the depolarization of the lidar return. Depolarizations of less than 3% indicate the presence of spherical water droplets. Depolarizations of greater than 23% indicate irregular ice particles. Identification of clouds with depolarization between 3% and 23% are less certain. These can be mixed phase clouds consisting of both ice and water, rain showers with large droplets, or certain ice crystal types that produce strong specular reflections from crystal faces. Very little rain falls in Eureka during this period, thus rain is not a major contributor. Also, the lidar points 4 degrees from the zenith to avoid strong specular reflection from oriented ice crystals. This plot will underestimate the optical depth contribution from dense clouds which completely extinguish the lidar beam. In Eureka, this typically occurs with low altitude water clouds where the HSRL return is lost before the optical depth reaches ~ 4.

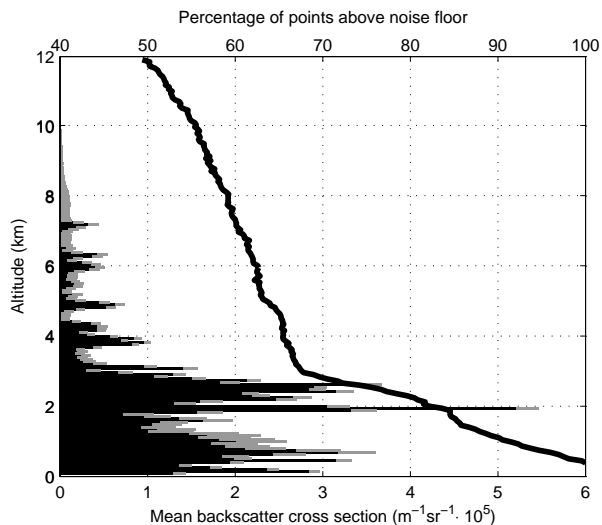Figure 2 shows that the clouds become less frequent and

Figure 5. Monthly mean backscatter cross section vs altitude for water (black bars) and ice (grey bars) and the percentage of lidar data points above the noise floor(black line). Data is for Eureka during August of 2005.
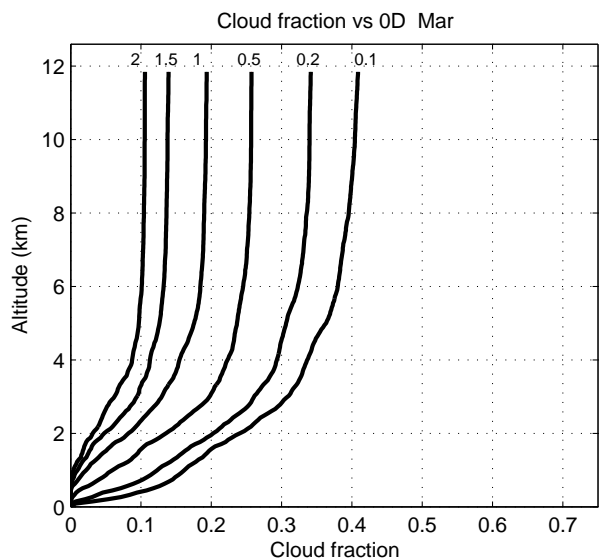

Figure 6. Cloud fraction as a function of altitude for March 2006 in Eureka. Curves show the fraction of the time that the atmosphere is clear up to a given altitude. Separate curves show the effect of changing the optical depth threshold which defines a cloud.

optically thinner during the winter. Figure 3 shows that the clouds change from predominately water in the late summer to predominately ice during the winter. This is not surprising considering that a typical wintertime surface temperature is -30 to -40 °C with an inversion temperature of around -20 °C.

Cloud climatologies often described cloud cover in terms of cloud fraction without specifying the threshold which distinguishes between cloudy and clear conditions. Figure 4 shows that cloud fraction is strong function of this threshold. Here we plot the fraction of the lidar profiles encountering a cloud as function of altitude above the lidar for the month of August, 2005 at Eureka. A profile is defined as cloudy when a threshold optical depth is reached. Separate curves are plotted for different thresholds. At 12 km, which is above all significant clouds at this location, the cloud fraction increases from 32% to 52% when the cloud threshold is decreased from optical depth 2 to optical depth 0.1.

Figure 5 shows the vertical variation in the monthly mean backscatter cross section for August 2005 at Eureka. Notice that low altitude water clouds and water fogs provide most of the optical depth with relatively small contributions from ice crystals. Higher altitudes are often obscured by low clouds.

Figure 6 shows the cloud fraction vs altitude and optical depth threshold for March 2006 in Eureka. The fractional cloudiness is much smaller than for August. The mean backscatter data for March (Fig. 7) shows a dramatic shift in cloud type relative to the August. With March surface temperatures often near $-40°$ C most of the scattering is due to ice crystals and often occurs in the form of ice fog or diamond dust precipitation.

Figure 8 shows the distribution of backscatter phase function values observed in ice clouds and ice precipitation during March of 2006 in Eureka. Ice crystals were selected by considering only those points where the lidar depolarization was greater than 25%. In order to reject points which were contaminated by noise, only points with a lidar signal-to-noise ratio of at least 5 and with a backscatter cross section greater than 10^{-5} $m^{-1}sr^{-1}$ were included. Data points below 1 km were also excluded to minimize errors in the measured scattering cross section caused by uncertainties in the lidar overlap correction. This result from the Arctic, showing a distribution that is sharply peaked at a value of $P(180)/4\pi = .036$ is nearly identical to the distribution measured over Madison, WI [8; 9]. This information will be useful in analyzing data from satellite borne lidars.

The utility of combining radar and lidar data is illustrated in Figure 9. Radar measured Doppler velocities are shown as a function of the lidar-radar derived effective diameter. Data has been combined into 60 meter altitude and 180 second time averages for August 2005 at Eureka. All points meeting a signal-noise-threshold with a backscatter cross section greater than 10^{-6} $m^{-1}sr^{-1}$ were used to create this contour plot. This lidar-radar size retrieval assumed solid ice spheres and a gamma distribution of particle sizes. The concentration of points centered on zero Doppler velocity with diameters less than 30 microns is readily identified with water clouds when the figure is re-plotted excluding points with depolarization < 20%. A 20% depolarization threshold also eliminates points in the region of 100 micron effective diameter and 1 m/sec fall velocities along with the small peak evident near 250 microns and 1.1 m/sec. These are
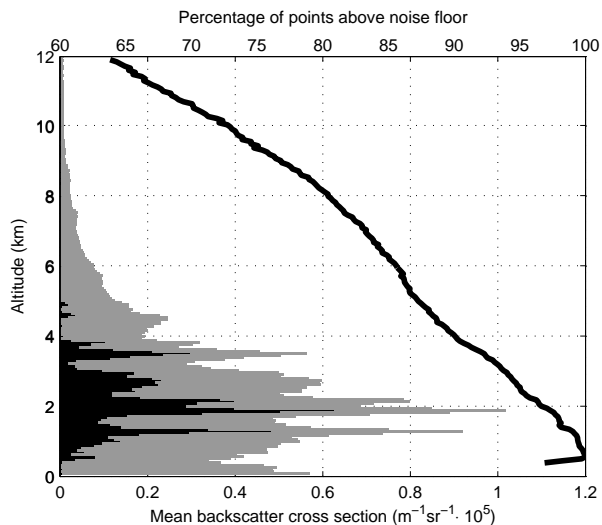
Figure 7. Monthly mean backscatter cross section for March 2006 in Eureka. Water contribution (black bars) and ice contribution (grey bars) with the black line showing the percentage of points above the noise floor.

Figure 9. Fall velocity as a function of particle effective diameter for August 2005. Contour show the number of cloudy data points where each point is a average over 3 minutes and 60 m of altitude. Data points with a signal-to-noise-ratio less than 2 are not plotted and a backscatter cross section threshold of $> 10^{-6}$ m^{-1}sr^{-1} is used to select cloudy data points.

associated with regions of high radar backscatter and are easily identified with periods of rain and drizzle that occurred on between Aug 19th and 23th. Variations in ice crystal shape pose a difficult problem for nearly all attempts to remotely characterize ice clouds. Further, investigation of particle fall velocity as a function of retrieved particle size may provide helpful constraints on the effects of particle shape.
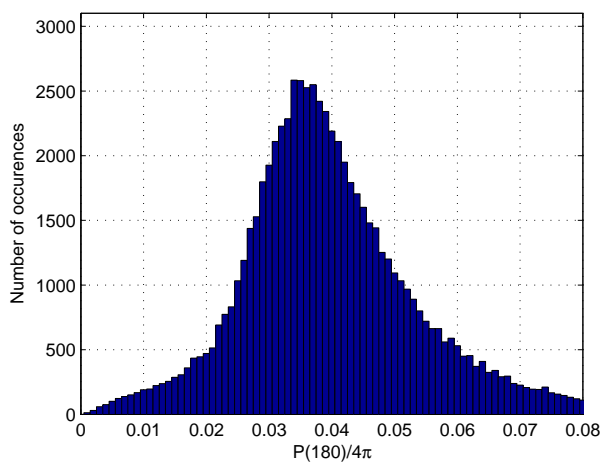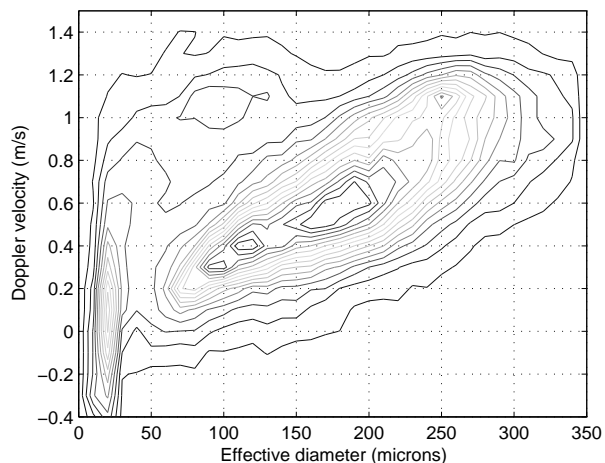
REFERENCES

[1] Knuteson, R. O., H. E. Revecomb, R. A. Best, N. C. Ciganovich, G. Dedecker, T. P. Dirkx, S. C. Ellington, W. F. Feltz, R. K. Garcia, H. B. Howell, W. Smith, J. f. Short and D. C. Tobin. Atmospheric Emitted Radiance Interferometer. *J. Atmos. Oceanic Technol.* 21(12), pp 1763-1776: 2004.

[2] Eloranta, E. W. High Spectral Resolution Lidar. *in Lidar: Range-Resolved Optical Remote Sensing of the Atmosphere*, Edited by C. Weitkamp, Springer-Verlag, New-York, 2005, 455p.

[3] Moran, K. P., B. E. Martner, M. J. Post, R. A. Kropfli, D. C. Welsh and K. B. Widener. An unattended cloud-profiling radar for use in climate research. *Bull. Amer. Meteor. Soc.* 79, 443-455, 1998.

[4] Donovan, D. P. and A. C. A. P. van Lammeren. Cloud effective particle size and water content profile retrievals using combined lidar and radar observations 1. Theory and examples. *J. Geophy. Res.* 106(D21), 27425-27448, 2001.

[5] Intrieri, J. M.,M. D. Shupe, T. Uttal, B. J. McCarty An annual cycle of Arctic cloud characteristics observed by radar and lidar at SHEBA. *J. Geophys. Res. (C Oceans)*, 107: 2002.

Figure 8. Backscatter phase function distribution for ice crystals measured during march, 2006. Data selected with depolarization $> 25\%$, altitude > 1 km, backscatter cross section $> 10^{-5}$ m^{-1}sr^{-1} and a lidar signal to noise ratio of > 5.

[6] Razenkov, I. A., E. W. Eloranta, J. P. Hedrick, R. E. Holz, R. E. Kuehn, and J. P. Garcia. A High Spectral Resolution Lidar Designed for Unattended Operation in the Arctic. *Proc. ILRC21, 57-60, 2002*

[7] Pirronen, P. A high spectral resolution lidar based on an iodine absorption filter Ph.D. thesis, Univ. of Joensuu, Joensuu, Finland, pp 113, 1994.

[8] Eloranta, E. W.,R. E. Kuehn, and R. E. Holz Measurements of backscatter phase function and depolarization in cirrus clouds made with the University of Wisconsin High Spectral Resolution Lidar. *Proc. ILRC20, 57-60, 2000* 255-257.

[9] R. E. Holz Measurement cirrus backscatter phase functions using a high spectral resolution lidar. University of Wisconsin-Madison MS Thesis, 2002, 67p.